Research Report 119

March, 1964

Dynamic Response of Snow to High Rates of Loading

by H. Napadensky

U.S. ARMY MATERIEL COMMAND
COLD REGIONS RESEARCH & ENGINEERING LABORATORY
HANOVER, NEW HAMPSHIRE

PREFACE

This is the final report on Armour Research Foundation Project D246, "Dynamic response of snow to high rates of loading". This work was done for the Applied Research Branch, Dr. A. Assur then Chief, under USA CRREL contract no. DA-11-190-ENG-127. This program was conducted during the period July 1961 to June 1962.

The experimental portion of this study, which was conducted at Camp Century, Greenland, during the summer of 1961, is described in detail in a Data Report issued in May 1962. Assistance in the analysis of the test records and computations was given by Mr. Richard H. Blumenthal.

This report has been reviewed and approved for publication by Headquarters, U. S. Army Materiel Command.

W. L. NUNGESSER
Colonel, CE
Commanding
USA CRREL

Manuscript received 27 January 1962

Department of the Army Task 8S-66-02-001-02

CONTENTS

	Page
Preface	ii
Summary	iv
Code index	v
Introduction	1
Experimental method	1
Data reduction	3
Determination of Hugoniot curves from experimental data	3
Determination of elastic-wave speed	4
Determination of particle velocity behind elastic wave	4
Determination of shock and particle velocities behind plastic wave	4
Sources of scatter in the results	19
Variations within any snow type	19
Errors in the data-reduction process	23
Errors associated with neglecting geometry changes	23
Conclusions and recommendations	23
References	25
Appendix A: Experimental procedures	A1

ILLUSTRATIONS

Figure		
1.	Sample streak camera record of dynamic response of TWH-23 snow	2
2.	Pressure as a function of specific volume curve for a medium that will support both an elastic and plastic shock wave	2
3.	Test arrangement	4
4.	Hugoniot curves for TWV-23, TWH-23, and MH-8 snow	5
5.	Hugoniot curves for NP and OP snow	5
6.	Hugoniot curves for TWV-16 and TWH-16 snow	5
7.	Bargraph method for estimating elastic-wave velocity	6
8-15.	Velocity curves used for calculation of Hugoniot equation	7, 8
16.	Hugoniot curve for Michigan snow	9
17.	Response of snow in the pressure vs particle-velocity plane	9
18.	Response of snow in the P_2 vs P_1 plane	10

TABLES

Table		
I.	Summary of initial parameters	11
II.	Experimental data and Hugoniot values	12
III.	Actual measured values of density and permeability for three samples of each snow type	21
IV.	Elastic-wave velocity as calculated from Young's modulus	22

SUMMARY

An experimental investigation of stress-wave propagation in snow and ice is described. Seven types of Greenland snow were investigated to determine the extent to which the variation in dynamic response of the snow is a function of snow types, and were compared with results of similar Michigan snow experiments. A low-density explosive charge was detonated, sending a steep-fronted shock wave through a metal transfer plate and into the snow sample, compressing the snow and setting it in motion. Measurements were made on shock waves with amplitudes of less than 200 atm. Density and pressure behind the wave fronts were determined by simultaneous measurement of wave-propagation and particle velocity as limited by the fast elastic wave and the slow plastic wave of the two-front structure. Values calculated by the Rankine-Hugoniot jump conditions determined the points at which the material behaves plastically or hydrodynamically. The maximum stable pressure-volume states that snow can reach under shock loading are also shown. Sources of scatter in the results from variations in snow type and errors in data reduction and geometry changes are pointed out.

CODE INDEX

The following codes are used to describe the various snow types investigated:

OP	Old Peter Snow
NP	New Peter Snow
MH-8	Middle Horizontal Core, 8-ft Depth
TWH-16	Trench Wall, Horizontal Core, 16-ft Depth
TWV-16	Trench Wall, Vertical Core, 16-ft Depth
TWH-23	Trench Wall, Horizontal Core, 23-ft Depth
TWV-23	Trench Wall, Vertical Core, 23-ft Depth

BLANK PAGE

DYNAMIC RESPONSE OF SNOW TO HIGH RATES OF LOADING

by

H. Napadensky

INTRODUCTION

This report describes an experimental investigation of stress-wave propagation in snow and ice. Since the behavior of materials under dynamic loading conditions cannot be reliably inferred from static experiments, the results of this study will help in filling the gap in the understanding of the behavior of snow and ice under shock or impact loading. The experiments, conducted on small samples, provided data from which the dynamic yield and the pressure at which the material behaves plastically or hydrodynamically were determined. Seven types of Greenland snow were investigated to ascertain the extent to which the variation in dynamic response of the snow is a function of snow types; the results for Greenland snow were compared with the results of several experiments on Michigan snow.

In the experiments, a low-density explosive charge was detonated in contact with a metal plate, giving rise to a steep-fronted shock wave in the plate. This shock wave was transmitted through the plate and into the snow sample, compressing the snow and setting it in motion. Measurements were made on shock waves with amplitudes of less than 200 atm. At these pressures a single shock front is unstable and splits into two fronts. The first wave travels at the elastic dilatational velocity and should have a stress amplitude equal to the elastic limit. This front is followed by the slower plastic shock wave which carries the material to the final pressure. The region between the two waves is substantially a constant state. Figure 1, a sample of an actual test record, shows the multiple-wave structure. Figure 2 is a schematic of a one-dimensional compression curve which represents the locus of pressure-volume states attainable with such a material.

The data showed the maximum stable pressure-volume states that snow can reach under shock loading. Data of this kind are required for estimating the yield of nuclear or chemical weapons, determining the size of a crater resulting from an explosion, detecting underground explosions, designing hardened or protective under-snow structures, and in solving problems which involve the impact of a projectile or the landing of an airplane on snow (Def. R and E Bulletin 29, 1961; Anderson, 1962; Chaszeyka, 1958 and 1961).

EXPERIMENTAL METHOD

The dynamic method used to determine stress and the corresponding compression requires the simultaneous measurement of wave-propagation velocity and particle velocity. In snow several waves are generally observed on the test records. These are bounded by the fast elastic wave and the slower plastic wave. The density and pressure, or compression and stress, behind the elastic and plastic waves can be calculated directly from the Rankine-Hugoniot jump conditons expressing conservation of mass and momentum. Across the elastic-wave front these relationships are:

$$P_1 = \rho_0 c_0 u_{p_1} \tag{1}$$

$$\rho_1 = \rho_0 c_0 / (c_0 - u_{p_1}) \ . \tag{2}$$

Across the plastic-wave front the following equations hold:

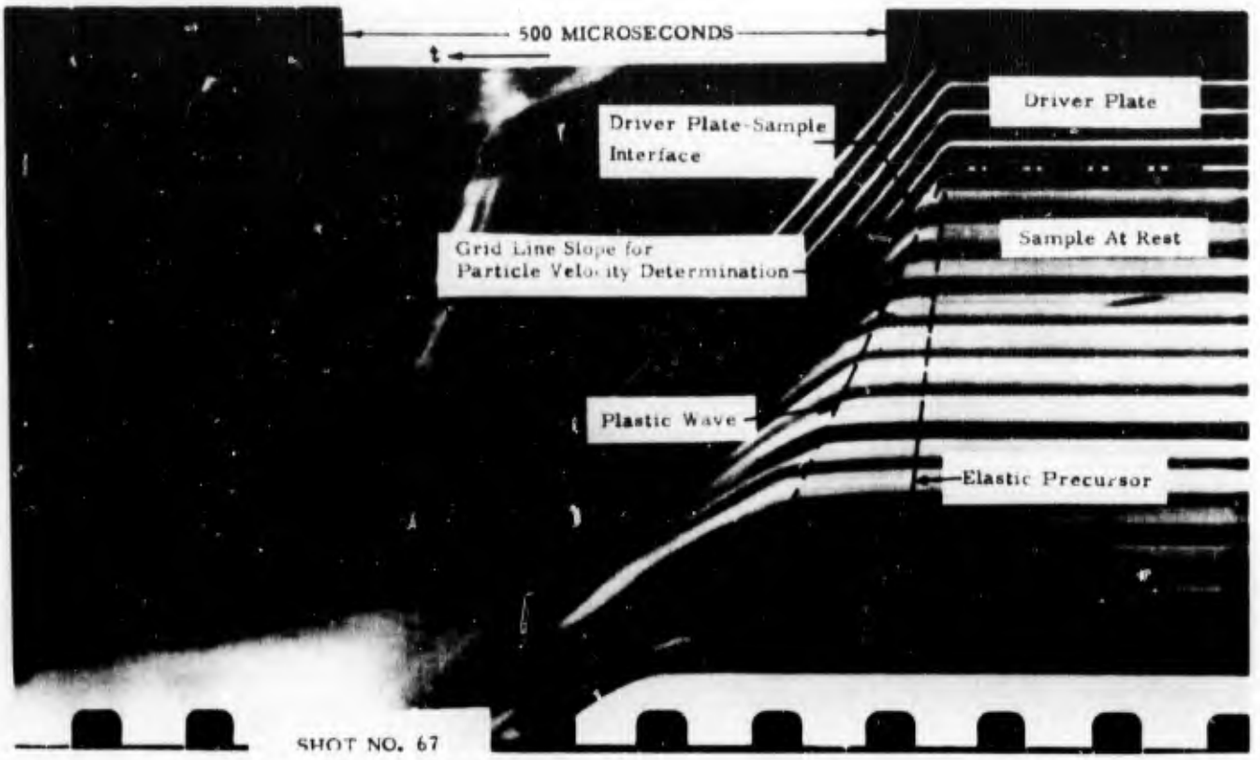

Figure 1. Sample streak camera record of dynamic response of TWH-23' snow.

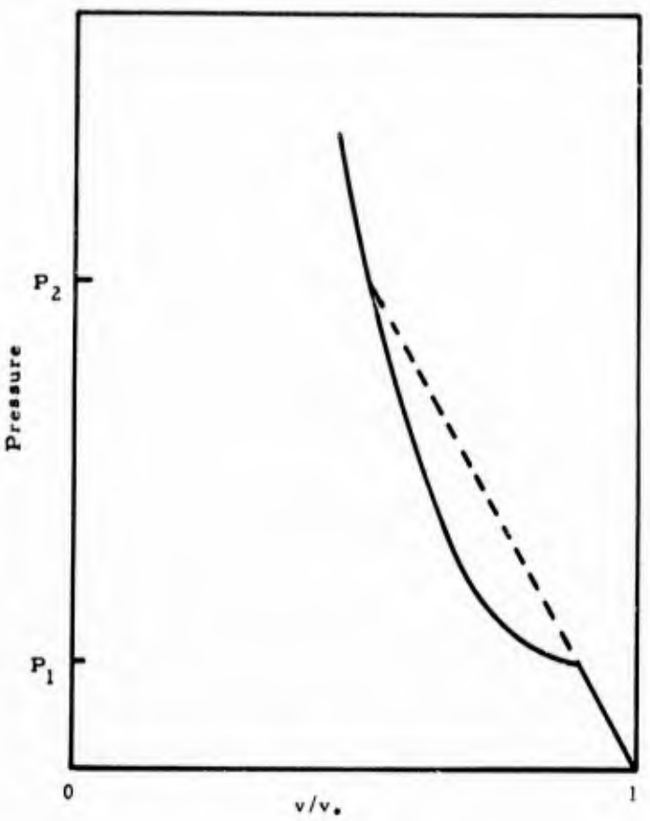

Figure 2. Pressure as a function of specific volume curve for a medium that will support both an elastic and plastic shock wave.

$$P_2 = P_1 + \rho_i (U_s - u_{p_1}) (u_{p_2} - u_{p_1}) \quad (3)$$

$$\rho_2 = \rho_1 (U_s - u_{p_1}) \Big/ (U_s - u_{p_2}) \quad . \quad (4)$$

Where: c_0 = the elastic-wave velocity

U_s = the wave velocity at which the plastic waves propagate

u_p = the particle velocity

ρ = the density

P = the pressure normal to the wave front, and

Subscript:

1 refers to the state ahead of the wave front

2 refers to the state immediately behind the front.

The experimental arrangement used to determine the wave velocities and corresponding particle velocities is shown in Figure 3. In each experiment, a metal driving plate was accelerated by a charge of low-density explosive. The plate compressed a cylinder of the material being investigated, and the motion of the plate was retarded by the resistance to compression of the specimen. A streak camera was used to record the motion of the plate and the horizontal lines of a reference grid which were stencilled on the curved surface of the specimen. The detonation of the explosive and the acceleration of the plate were so nearly instantaneous that the acceleration time was barely resolved by the streak camera. The propagation of compression waves through the specimen can be seen as the progressive displacement of the reference lines painted on the edge of the specimen.

Table I summarizes the initial loading conditions for the test records that were analyzed. A detailed description of the experimental procedure and a record of each experiment are found in Napadensky (1962). An abstract of the experimental procedure is given in Appendix A.

Data reduction

Inasmuch as a large number of experiments were performed, it was desirable to make the data reduction as routine as possible. At first an automatic digital-data reader was used to obtain the (x, t) information from the streak records. The reader had two movable hairlines which permitted the simultaneous determination of x (vertical distance)and t (time) coordinates of any point on the record. The output was fed directly to a typewriter and a punched paper tape. Although this method of data reduction is very attractive, it had to be abandoned because of the intermittent drifting of the $x = 0$ axis. The method finally used for determining particle velocities was to measure the slope of each of the reference lines painted on the specimen. The compression-wave or shock-wave velocity in the snow was determined by measuring the slope of the line which is the locus of points representing the time of the initial movement of the reference grid.

The actual computations for determining velocities, pressures, and densities were performed on the Armour Research Foundation UNIVAC 1105 computer.

DETERMINATION OF HUGONIOT CURVES FROM EXPERIMENTAL DATA

The pressure-volume relationships (the Hugoniot) plotted in Figures 4-6 were obtained from measurements of the velocities of the elastic wave, plastic wave, and particles and through application of eq 1, 2, 3, and 4.

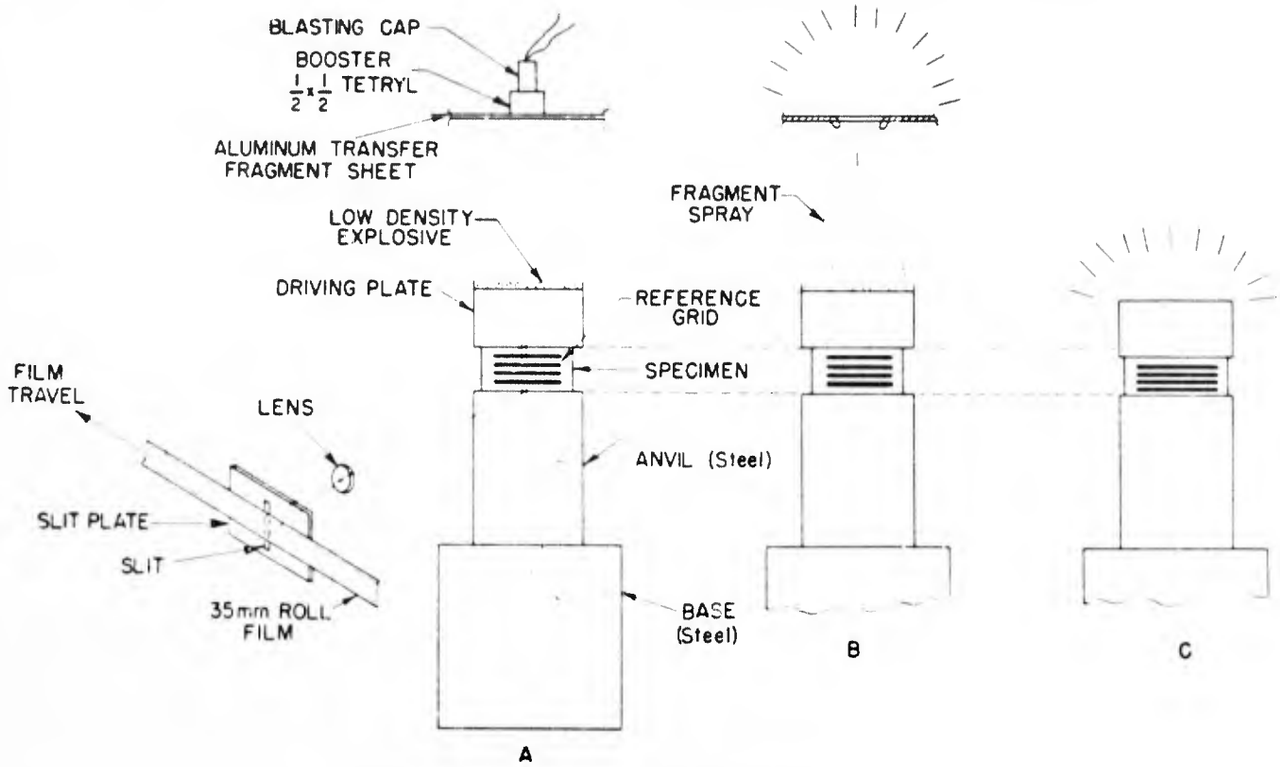

Figure 3. Test arrangement.

Determination of elastic-wave speed

Since there was, for most of the snow types, considerable variation in the calculated elastic-wave velocity, and since these variations seemed to be random and could not be correlated with any parameter, it was decided to assume a constant value for the elastic-wave velocity. The value of the elastic-wave velocity used in the calculations of the pressure-volume relationships was determined by plotting, in bargraph form, the number of experiments which yielded a velocity falling within a certain velocity range against the computed elastic-wave velocity. This graph is shown in Figure 7. The most likely velocity of the elastic wave was estimated from this graph. The elastic-wave velocity determined by a vibrating beam method (Nakaya, 1959) is also indicated in Figure 7.

Determination of particle velocity behind elastic wave

The particle velocity behind the elastic wave (u_{p_1}) was taken as the average of all the v_1 and v_2 values listed in Table II. The average was used since confidence in the accuracy of v_1 was not high as the line segment on the test record which represents v_1 was generally small in length. It was also expected that the value of v_2 should be close to v_1.

Determination of shock and particle velocities behind plastic wave

The values of plastic-wave velocity and particle velocity (or velocity at the snow-driver plate interface), as tabulated in Table II, are plotted in Figures 8-14 for each type of snow investigated. A smooth curve was drawn through these points. The values of U_s and u_{p_2} taken off the smoothed curve were used in the calculations of the pressure-volume relationships across the plastic-wave front.

Table II also lists the P-V (or P-ρ_0/ρ) relationships across the elastic and plastic waves, as computed from the raw data, prior to the smoothing methods just described. The curves in Figures 4-6 are the results of computations on points from the smoothed velocity curves of Figures 8-14. The solid lines on the P-V curves are for actual data points. The dashed line on the curve represents the results of computations based on an extrapolation of the shock velocity-particle velocity curves of Figures 8-14.

Several preliminary experiments were conducted in Chicago on Northern Michigan snow of density 0.5 g/cm^3. The results of the analysis can be seen in Figures 15 and 16.

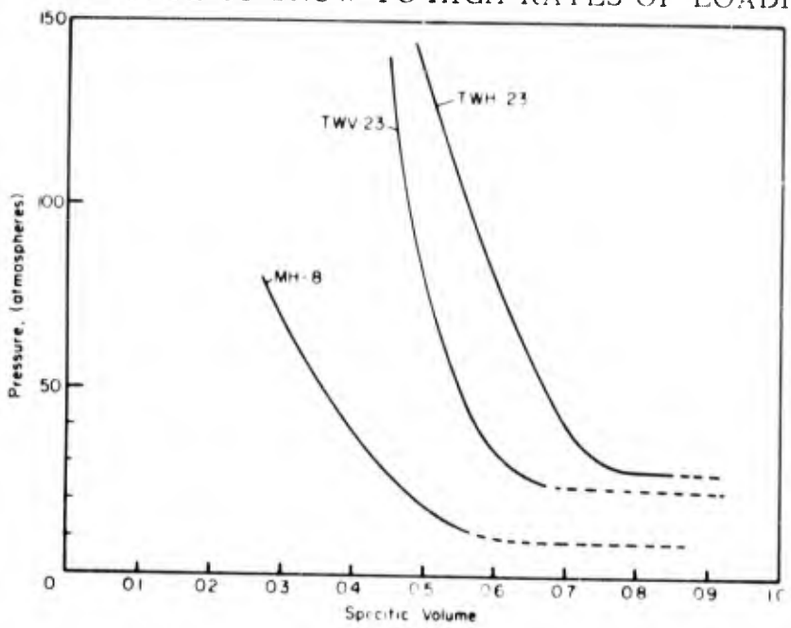

Figure 4. Hugoniot curves for TWV-23, TWH-23, and MH-8 snow.

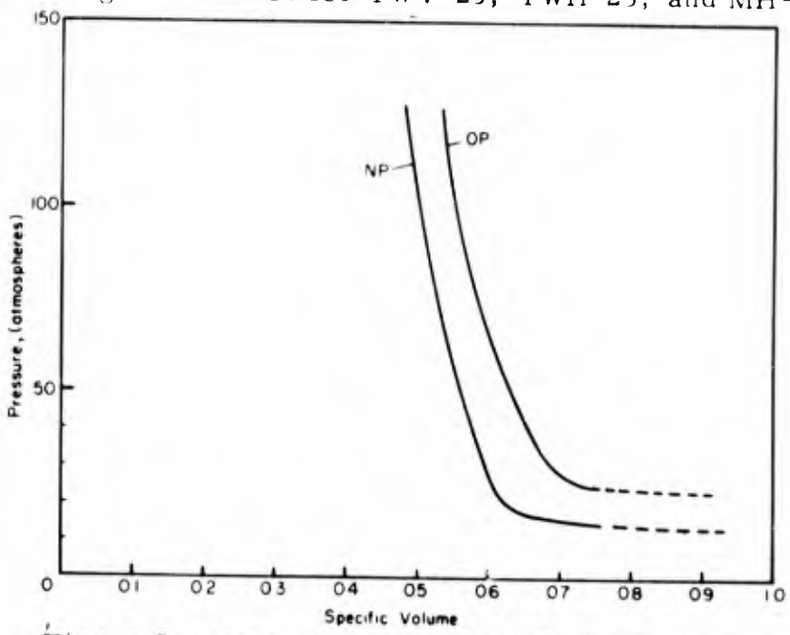

Figure 5. Hugoniot curves for NP and OP snow.

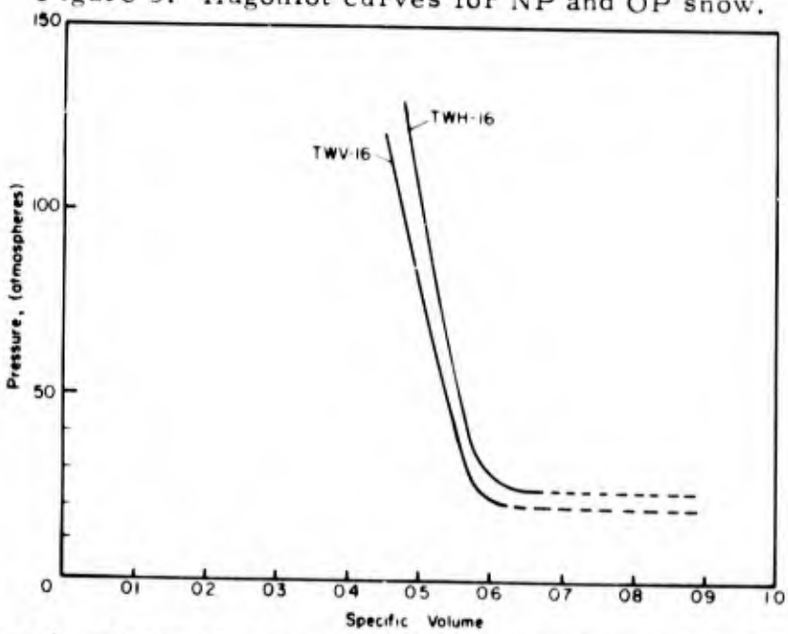

Figure 6. Hugoniot curves for TWV-16 and TWH-16 snow.

Finally, Figures 17 and 18 show individual plots of pressure versus particle velocity and the relation of stresses across the elastic- and plastic-wave fronts. There are distinct groups with different characteristics. This behavior may warrant further study. Similar groups can be plotted for the other types of snow based upon the data in Table II.

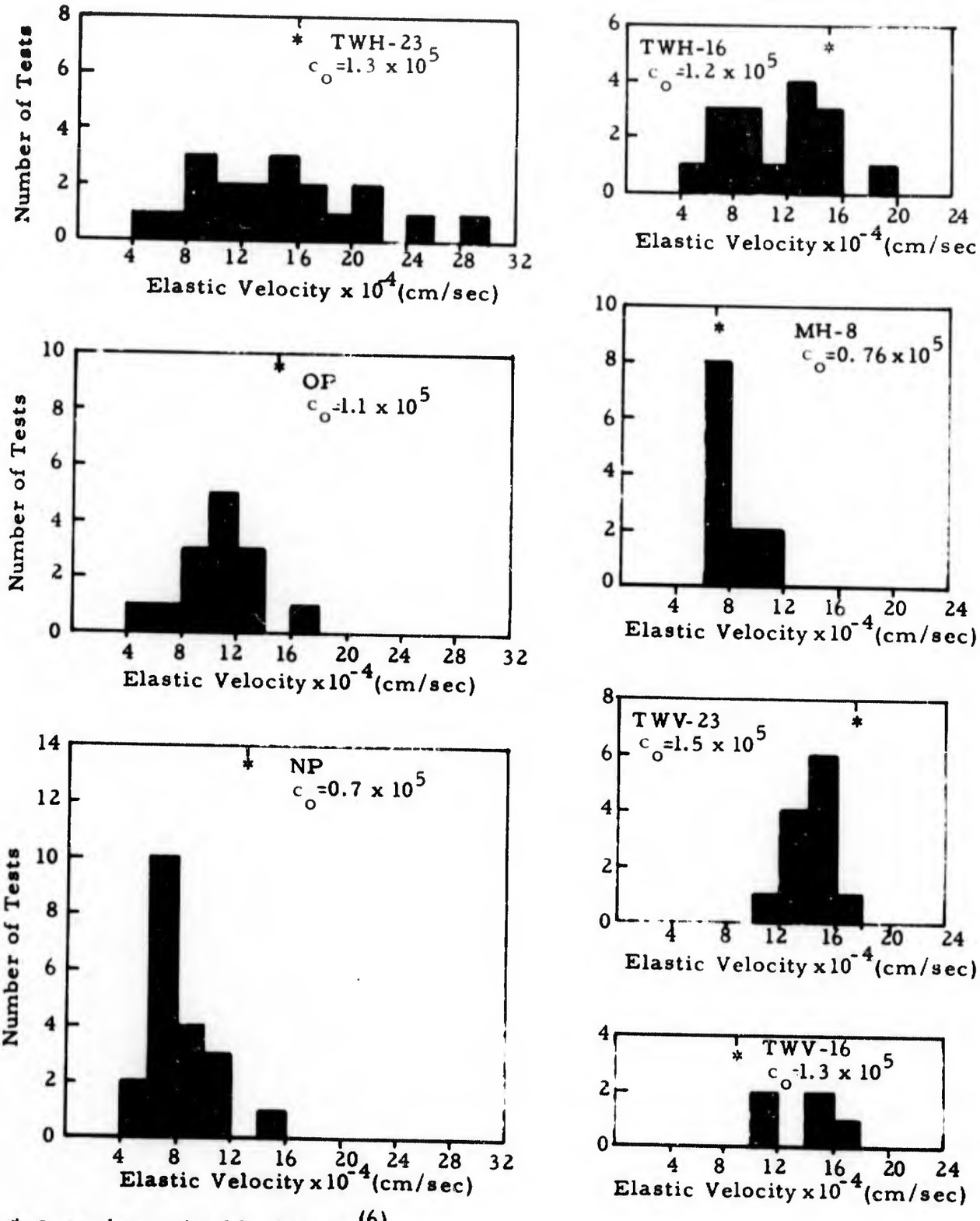

* c_o as determined by Nakaya[6]

Figure 7. Bargraph method for estimating elastic-wave velocity.

BLANK PAGE

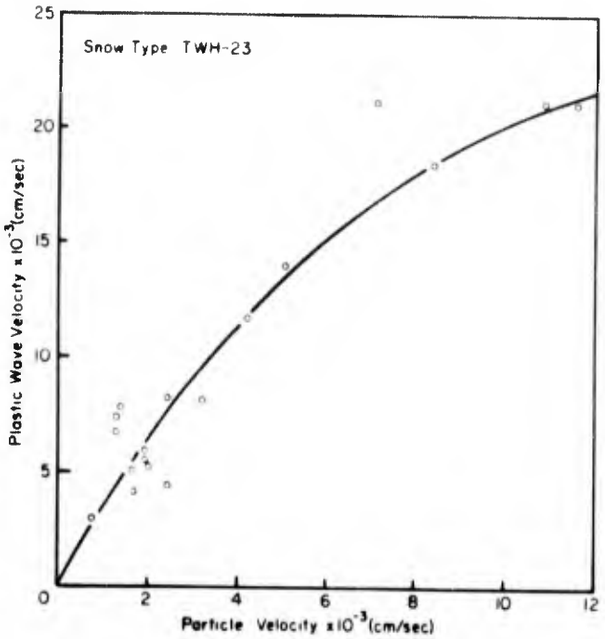

Figure 8. Velocity curve used for calculation of Hugoniot equation of state of TWH-23 snow.

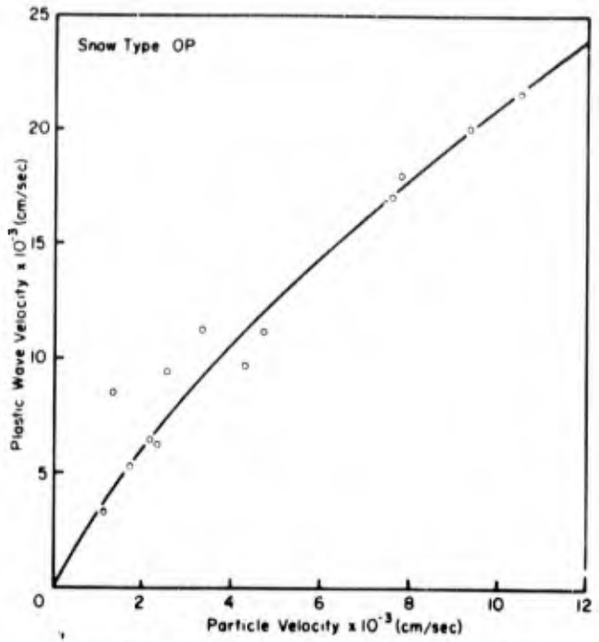

Figure 9. Velocity curve used for calculation of Hugoniot equation of state of OP snow.

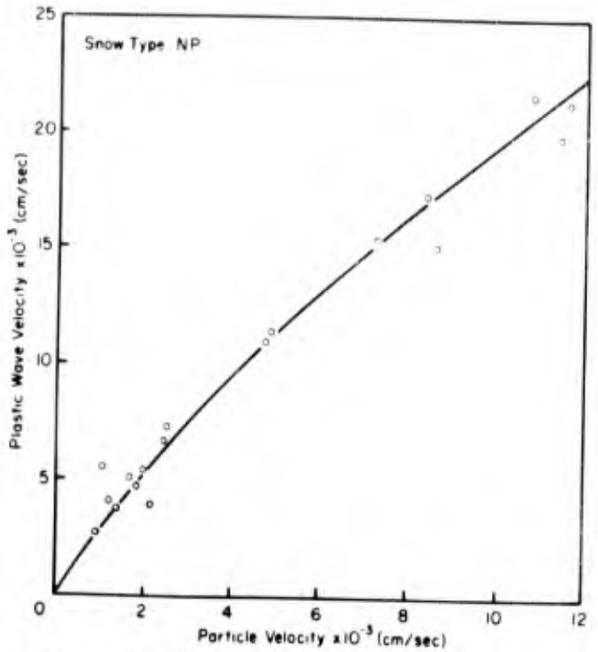

Figure 10. Velocity curve used for calculation of Hugoniot equation of state of NP snow.

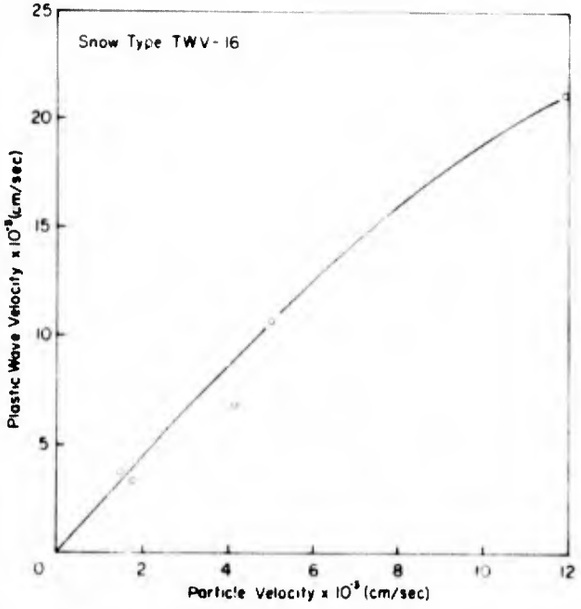

Figure 11. Velocity curve used for calculation of Hugoniot equation of state of TWH-16 snow.

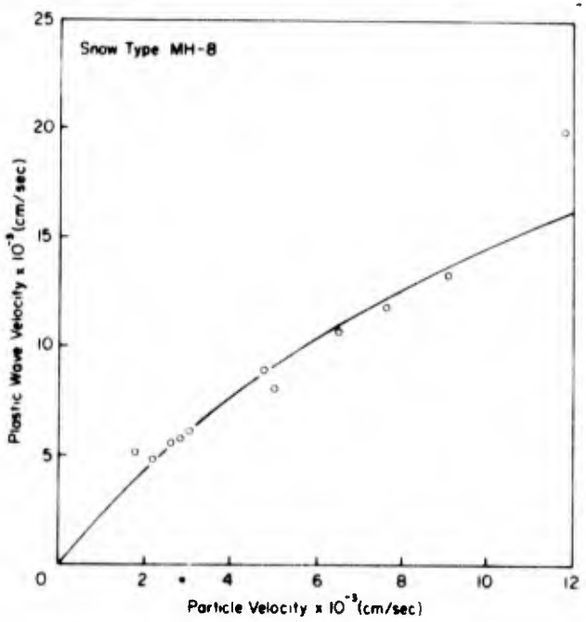

Figure 12. Velocity curve used for calculation of Hugoniot equation of state of MH-8 snow.

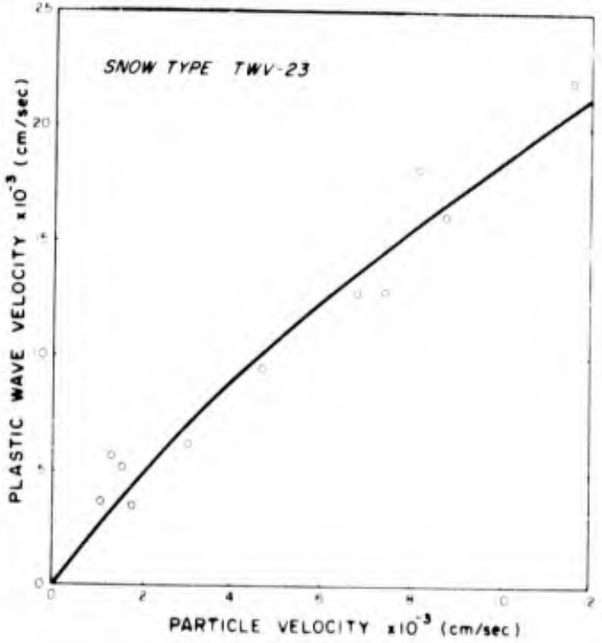

Figure 13. Velocity curve used for calculation of Hugoniot equation of state of TWV-23 snow.

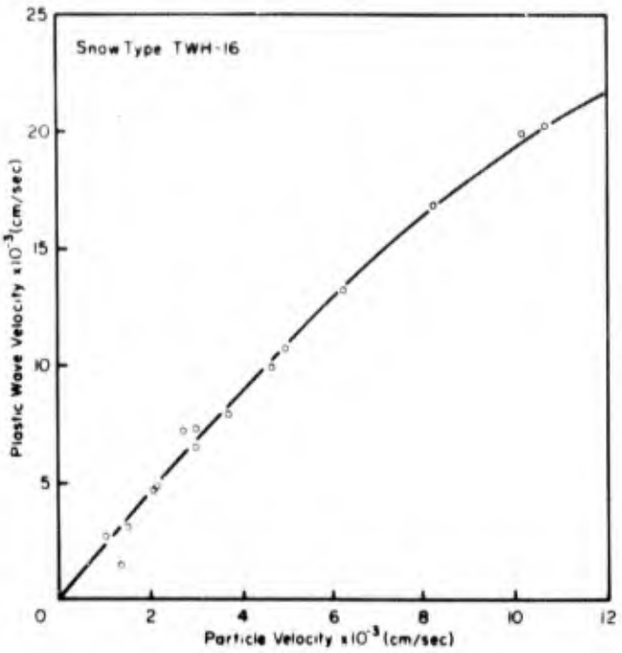

Figure 14. Velocity curve used for calculation of Hugoniot equation of state of TWV-16 snow.

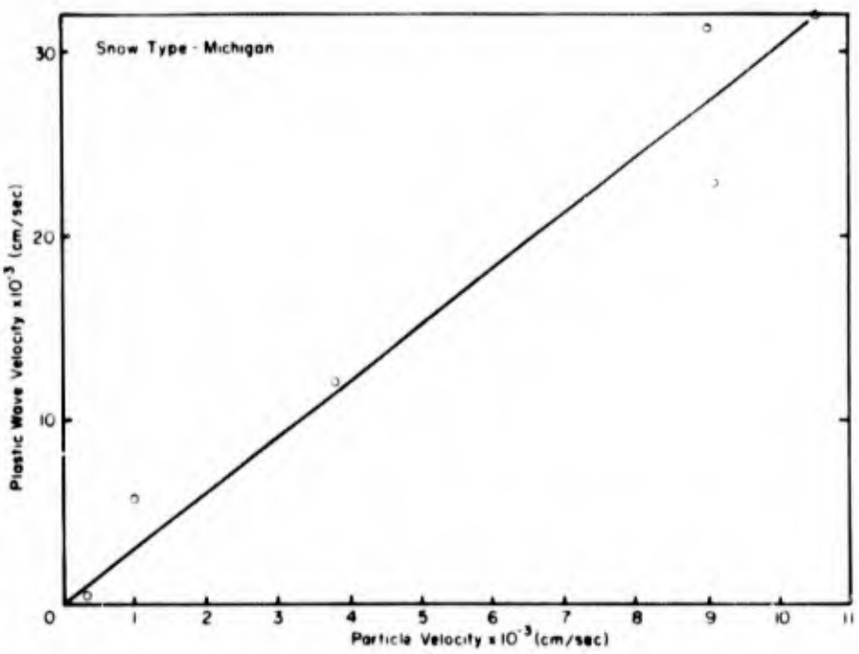

Figure 15. Velocity curve used for calculation of Hugoniot equation of state of Michigan snow.

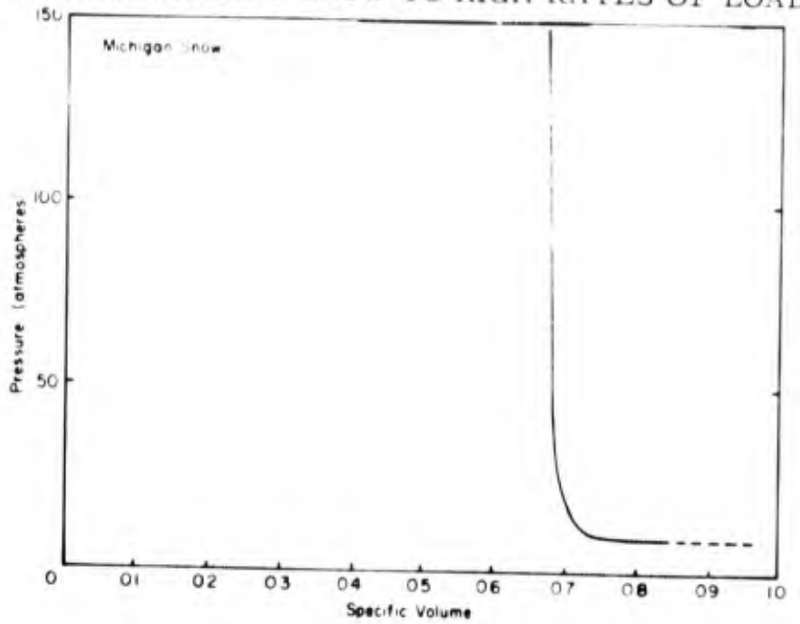

Figure 16. Hugoniot curve for Michigan snow.

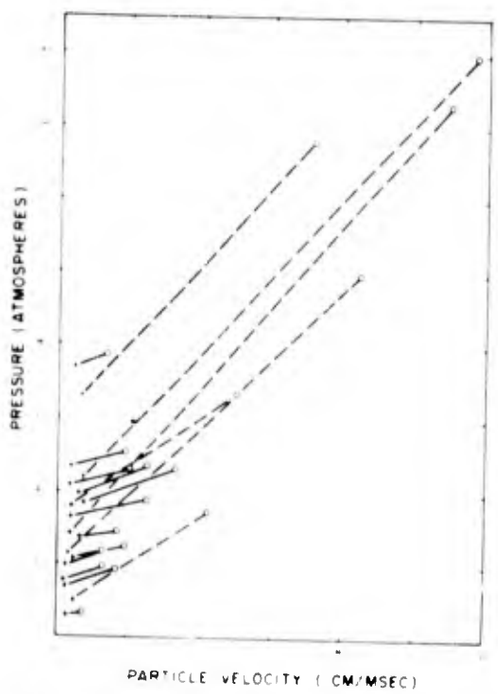

Figure 17. Response of snow in the pressure vs particle-velocity plane. (Snow type TWH-23)

This graph illustrates the dependence of the stress in the first wave upon the stress in the second wave. The points indicated by crosses, +, refer to the state of stress across the first wave or elastic wave. The points indicated by circles, o, refer to the state of stress across the second wave or plastic wave. For each experiment a continuous or a dashed line is drawn connecting these two points. The continuous lines represent those experiments where the jump in stress from elastic to plastic behavior is small. The dashed lines represent those experiments for which the jump in stress from elastic to plastic behavior is large.

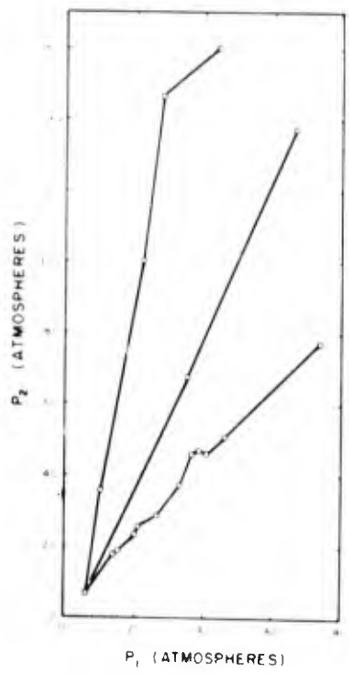

Figure 18. Response of snow in the P_2 vs P_1 plane. (Snow type TWH-23)

This graph illustrates the correlation between the stress in the first wave and the stress in the second wave.

P_1 represents the stress across the elastic wave front.

P_2 represents the stress across the plastic wave front.

These curves correspond, roughly, to the family of continuous lines and dashed lines of Figure 17.

BLANK PAGE

Table I. Summary of initial parameters.

INITIAL LOADING CONDITIONS				SNOW TYPE						
Driver plate			Explosive	TWH-23 Record number*	OP Record number*	NP Record number*	TWH-16 Record number*	MH-8 Record number*	TWV-23 Record number*	TWV-16 Record number*
Material	Diam (cm)	Ht (cm)	Wt (g)							
Steel	6.35	10.16	20	1, 17, 19 165, 169, 170	27, 35 49	53, 88	69, 79 93, 141	99	133	155
Steel	6.35	10.16	30	2, 12, 23 166	28, 45	57, 86	77, 143		127 138	156
Steel	6.35	7.62	30	3, 10	29, 38 50	54, 56 60, 83	71, 73 148	109	126 132	164
Steel	6.35	6.35	30	4, 11, 14 24		62, 87	74, 144	101, 107 114	119 131	158
Steel	6.35	6.35	40	5, 26	31, 37 43	51, 66 84	70, 96 145	116	123 134	157
Steel	6.35	6.35	50				97, 140	100, 118	120 137	160
Alum.	6.35	5.08	20	6, 9, 21	39, 46	55, 61 85	72, 80 94, 139	106, 112	121	159
Alum.	6.35	5.08	30				98	104, 115	125 135	154
Alum.	6.35	5.08	40	7, 20	33, 41 47	52, 64 89	68, 78	108	128 129	
Alum.	6.35	4.13	50	13, 18, 22	36, 44	58, 63 90	67, 95 146	102, 110	136	153

*Records obtained only.

Table II a. Experimental data and Hugoniot values.

Snow type TWH-23; $\rho_0 = 0.528\ g/cm^3$; Permeability = 58 cm/sec

Record number	Temp (C)	Impact velocity (cm/sec)	Plastic velocity (cm/sec)	Elastic velocity (cm/sec)	Particle velocities behind elastic wave (cm/sec)				P_1 (bars)	ρ_0/ρ_1	P_2 (bars)	ρ_0/ρ_2
					V_1	V_2	V_3	V_4				
1	-12.8	745	2,970	40,200	289	248	165	–	6.14	0.992	6.8	0.825
2	-12.8	1,290	7,430	114,000	248	99	–	5	14.9	0.998	18.8	0.855
3	-12.2	1,660	5,080	110,000	240	240	–	–	14.0	0.998	18.4	0.672
4	-12.2	1,690	4,050	72,600	696	306	306	–	26.7	0.990	28.5	0.698
5	-11.1	3,210	8,120	93,500	745	465	186	–	36.8	0.992	46.5	0.662
7	-11.1	7,100	21,300	181,000	694	521	289	–	66.3	0.996	136.2	0.686
9	-12.2	5,080	14,000	167,000	403	461	307	–	35.7	0.997	67.6	0.655
10	-13.3	1,940	5,530	206,000	428	272	272	194	46.4	0.998	50.5	0.702
11	-14.4	2,440	4,470	172,000	363	474	316	316	33.1	0.998	37.6	0.494
12	-13.9	1,360	7,940	291,000	479	302	213	124	73.6	0.998	77.07	0.899
13	-13.9	10,900	21,600	152,000	352	352	352	352	28.2	0.998	146.6	0.503
14	-13.3	2,020	5,250	219,000	360	288	198	198	41.6	0.998	45.9	0.655
18	-11.1	12,500	21,800	255,000	–	374	327	218	–	1.000	143.5	0.427
20	-13.9	8,430	18,400	124,000	342	298	256	–	22.4	0.997	99.5	0.553
21	-12.8	4,210	11,700	151,000	128	410	547	256	10.2	0.999	35.2	0.647
22	- 7.8	11,600	21,300	84,900	989	574	359	269	44.4	0.988	159.5	0.471
23	- 7.2	1,300	6,790	142,000	266	258	121	–	19.9	0.998	23.5	0.842
24	- 7.2	1,940	5,970	80,900	485	472	525	–	20.7	0.994	25.0	0.732
26	- 7.2	2,440	8,260	130,000	568	485	451	401	39.1	0.996	46.7	0.755

Table II b. Experimental data and Hugoniot values.

Snow type OP; $\rho_0 = 0.505$ g/cm^3; Permeability = 80 cm/sec.

Record number	Temp (C)	Impact velocity (cm/sec)	Plastic velocity (cm/sec)	Elastic velocity (cm/sec)	Particle velocities behind elastic wave (cm/sec)				P_1 (bars)	ρ_0 / ρ_1	P_2 (bars)	ρ_0 / ρ_2
					V_1	V_2	V_3	V_4				
28	-15.0	1,110	3,350	122,000	134	75	60	–	8.3	0.999	9.9	0.696
29	-15.5	1,340	8,560	178,000	224	134	–	–	20.2	0.999	24.9	0.866
31	-15.0	2,570	9,450	103,000	413	346	313	–	21.4	0.996	31.3	0.758
33	-15.5	7,810	18,000	99,000	837	727	523	–	41.9	0.992	102.8	0.589
36	-17.8	10,500	21,700	105,000	796	760	601	565	42.2	0.992	142.5	0.531
37	- 9.4	3,360	11,700	111,000	197	157	147	–	11.0	0.998	29.4	0.726
38	-10.0	1,720	5,330	56,900	556	225	180	105	15.9	0.990	18.7	0.750
39	- 8.3	4,730	11,200	60,800	448	448	298	433	13.7	0.993	37.1	0.599
43	- 8.3	2,360	6,310	119,000	197	157	147	–	20.4	0.997	26.5	0.660
44	- 8.3	12,400	24,500	127,000	990	737	470	–	63.5	0.992	208.5	0.511
45	-10.6	1,270	3,910	139,000	213	178	195	213	14.9	0.998	16.9	0.714
46	-11.7	4,310	9,720	93,000	243	243	357	486	11.4	0.997	30.4	0.569
47	- 7.8	7,620	17,100	80,500	666	399	325	–	27.1	0.992	85.2	0.572
50	-10.6	2,180	6,470	112,000	539	470	392	352	30.5	0.995	35.5	0.722

Table II c. Experimental data and Hugoniot values.

Snow type NP; $\rho_0 = 0.499$ g/cm^3; Permeability = 36.9 cm/sec

Record number	Temp (C)	Impact velocity (cm/sec)	Plastic velocity (cm/sec)	Elastic velocity (cm/sec)	Particle velocities behind elastic wave (cm/sec)				P_1 (bars)	ρ_0 / ρ_1	P_2 (bars)	ρ_0 / ρ_2
					V_1	V_2	V_3	V_4				
51	- 8.9	2,500	7,310	71,800	316	289	253	235	11.3	0.996	18.9	0.685
52	- 8.3	7,230	15,400	61,500	686	404	510	387	21.0	0.989	69.5	0.551
53	- 9.4	919	2,710	74,700	212	212	212	229	7.9	0.997	8.8	0.717
54	- 8.3	1,690	5,080	112,000	436	401	348	–	24.3	0.996	27.2	0.727
55	-11.1	4,870	11,400	69,800	508	474	321	304	17.7	0.993	41.7	0.584
56	-11.1	1,850	4,840	64,700	477	159	127	95	15.4	0.993	19.9	0.616
57	-12.8	1,190	4,040	103,000	313	174	35	–	16.1	0.997	17.7	0.764
58	-12.8	10,800	21,700	66,300	557	372	321	321	18.5	0.992	119.4	0.513
61	-12.2	4,790	11,000	77,800	480	412	326	326	18.6	0.994	41.4	0.590
62	-12.2	1,980	5,430	60,400	225	155	–	–	6.7	0.996	11.3	0.663
63	-10.6	11,400	19,900	73,000	225	204	186	–	9.3	0.997	120.2	0.432
64	–	8,390	16,300	62,400	349	349	218	–	10.9	0.994	74.7	0.499
66	-11.7	1,040	5,590	52,400	155	121	–	–	4.1	0.997	6.4	0.837
83	-10.0	1,810	4,700	142,000	260	260	260	–	18.4	0.998	22.0	0.634
84	-12.8	2,450	6,670	83,900	524	402	349	297	22.0	0.994	27.9	0.687
85	-13.4	5,110	11,900	94,000	374	357	357	303	17.5	0.996	44.9	0.589
86	-13.4	1,350	3,810	97,400	164	164	131	65	7.9	0.998	10.11	0.675
87	-17.8	2,150	3,860	90,400	291	194	174	155	13.1	0.997	16.4	0.480
89	-16.7	8,610	15,100	105,000	604	403	329	201	31.7	0.994	89.9	0.466
90	-16.7	11,600	21,400	58,000	–	–	–	–		1.000	123.9	0.458

Table II d. Experimental data and Hugoniot values.

Snow type TWH-16; ρ_0 = 0.512 g/cm^3; Permeability = 85 cm/sec

Record number	Temp (C)	Impact velocity (cm/sec)	Plastic velocity (cm/sec)	Elastic velocity (cm/sec)	Particle velocities behind elastic wave (cm/sec)				P_1 (bars)	ρ_0/ρ_1	P_2 (bars)	ρ_0/ρ_2
					V_1	V_2	V_3	V_4				
69	-11.1	1,000	2,740	158,000	196	143	89	–	15.9	0.999	17.0	0.683
70	-11.1	2,740	7,190	82,200	493	365	183	–	20.7	0.994	28.4	0.661
71	-10.5	1,330	1,510	77,800	350	–	–	–	14.0	0.995	14.6	0.684
72	- 9.4	4,950	10,700	112,000	350	122	175	175	20.1	0.997	44.6	0.555
73	-10.0	1,490	3,120	68,100	133	133	120	–	4.7	0.998	6.7	0.545
77	- 8.9	1,340	2,570	131,000	138	138	–	–	9.3	0.999	10.8	0.506
78	-13.4	8,290	16,800	146,000	730	645	271	169	54.6	0.995	87.7	0.529
80	-10.0	4,630	9,880	57,100	403	363	363	–	11.8	0.993	32.5	0.551
95	-16.7	10,200	19,900	133,000	610	469	394	319	41.6	0.995	136.6	0.524
97	-16.7	3,010	7,240	132,000	284	246	208	189	19.2	0.998	29.0	0.607
98	-16.7	6,290	13,200	78,400	370	222	185	204	14.9	0.995	54.0	0.538
139	-14.4	3,010	6,440	190,000	371	297	167	–	36.1	0.998	44.1	0.564
140	- 3.9	3,700	7,940	155,000	188	188	146	146	14.9	0.999	28.9	0.547
144	-11.1	2,130	4,840	88,100	149	112	93	–	6.7	0.998	11.5	0.576
145	-11.7	2,070	4,770	98,100	298	139	112	139	14.9	0.997	18.0	0.601
146	-12.2	10,700	20,200	129,000	315	130	93	20	20.8	0.998	126.8	0.476

Table II e. Experimental data and Hugoniot values.

Snow type MH-8; ρ_0 = 0.388 g/cm³; Permeability = 18.5 cm/sec

Record number	Temp (C)	Impact velocity (cm/sec)	Plastic velocity (cm/sec)	Elastic velocity (cm/sec)	Particle velocities behind elastic wave (cm/sec)				P_1 (bars)	ρ_0 / ρ_1	P_2 (bars)	ρ_0 / ρ_2
					V_1	V_2	V_3	V_4				
100	-17.2	2,840	5,710	66,900	370	259	74	37	9.6	0.994	14.8	0.535
101	-16.7	2,190	4,800	105,000	180	198	216	180	7.4	0.998	11.0	0.562
102	-16.2	12,700	17,400	79,400	526	403	333	140	16.2	0.993	96.2	0.277
104	-14.4	7,650	11,800	66,200	531	300	177	124	13.6	0.992	44.9	0.366
106	-17.2	5,030	8,000	61,600	–	–	–	–	–	1.000	15.6	0.371
107	-15.6	2,630	5,480	63,600	356	71	71	–	8.7	0.994	13.3	0.553
108	-15.6	9,130	14,300	79,300	506	337	187	75	15.6	0.994	62.0	0.374
109	-17.8	1,810	5,160	88,600	304	215	125	90	10.4	0.997	13.3	0.688
110	-17.8	11,900	19,900	103,000	620	328	310	218	24.7	0.994	109.3	0.413
112	-18.9	4,780	8,930	81,900	128	73	73	–	4.1	0.998	20.0	0.472
115	-16.7	6,560	10,700	65,900	463	214	107	–	11.8	0.993	36.2	0.401
118	-15.0	3,030	6,070	63,800	229	132	106	–	5.7	0.996	12.1	0.520

Table II f. Experimental data and Hugoniot values.

Snow type TWV-23; ρ_0 = 0.529 g/cm³; Permeability = 30.2 cm/sec

Record number	Temp (C)	Impact velocity (cm/sec)	Plastic velocity (cm/sec)	Elastic velocity (cm/sec)	Particle velocities behind elastic wave (cm/sec)				P_1 (bars)	ρ_0/ρ_1	P_2 (bars)	ρ_0/ρ_2
					V_1	V_2	V_3	V_4				
120	-15.6	3,000	6,200	150,000	412	412	300	–	32.7	0.997	42.5	0.553
121	-16.7	4,650	9,510	152,000	389	–	241	148	31.8	0.997	52.4	0.532
125	-16.7	7,370	12,900	133,000	201	146	119	–	14.2	0.998	62.5	0.434
126	-16.7	1,730	3,510	129,000	235	217	181	181	16.0	0.998	18.6	0.543
127	-16.7	1,520	5,150	137,000	452	–	268	–	32.8	0.997	35.5	0.770
128	-16.7	8,750	16,200	143,000	430	197	286	134	32.5	0.997	102.1	0.472
129	-16.7	8,130	18,200	128,000	385	–	220	137	26.0	0.997	99.1	0.564
133	-12.2	1,020	3,750	165,000	186	146	93	–	16.2	0.999	17.8	0.764
134	-12.2	2,340	5,720	106,000	231	196	160	–	13.0	0.998	19.1	0.615
135	-11.7	6,790	12,800	145,000	199	127	181	–	15.2	0.999	59.2	0.476
136	-11.1	11,600	22,100	159,000	666	444	222	222	56.1	0.996	180.8	0.488
138	-12.2	1,266	5,644	159,811	74	93	148	4	32.7	0.999	36.3	0.785

Table II g. Experimental data and Hugoniot values.

Snow type TWV-16; $\rho_0 = 0.466$ g/cm^3; Permeability = 17.6 cm/sec

Record number	Temp (C)	Impact velocity (cm/sec)	Plastic velocity (cm/sec)	Elastic velocity (cm/sec)	Particle velocities behind elastic wave (cm/sec)				P_1 (bars)	ρ_0 / ρ_1	P_2 (bars)	ρ_0 / ρ_2
					V_1	V_2	V_3	V_4				
153	-11.1	12,000	21,100	109,000	–	203	–	147	–	1.000	120.0	0.436
154	-11.1	6,680	14,600	113,000	476	33	229	–	25.1	0.996	66.2	0.558
156	-11.7	1,490	3,770	237,000	253	253	217	271	28.0	0.999	30.0	0.640
159	-11.7	5,010	10,700	153,000	328	300	281	337	23.5	0.998	46.4	0.543
160	-10.6	4,130	6,740	169,000	817	185	111	111	64.2	0.995	73.1	0.452
164	-11.1	1,740	3,340	144,000	456	333	298	123	30.6	0.997	32.3	0.555

BLANK PAGE

SOURCES OF SCATTER IN THE RESULTS

Many factors contribute to the scatter in the data on the response of snow. These factors can be divided into two categories. In the first group are the variations associated with the test itself; that is, the variations in the physical properties within any one snow type, variations in the temperature of the cold room and of the trench, and variations in the initial loading conditions. In the second group are the errors associated with the data reduction process. It is possible to estimate the effect of these several sources of variations on the measured values of velocity.

Variations within any snow type

The influence of variations in initial density. Several parameters were measured to characterize the initial state of the snow. These quantities were the depth below the surface from which the core was taken; the orientation of the core, whether horizontal or vertical; the density of the snow; and the permeability of the snow. Although the logbook (Napadensky, 1962) shows only one value for density and one value for permeability for each snow type, these values were based on the average of three measurements for each snow type. The actual measurements are shown in Table III. This table shows that the density variations within most of the snow types are large. Thus, it is important to ascertain the extent of the dependence of the wave-propagation velocities on the density. The influence of the density parameter can be estimated by reference to Nakaya (1959) who, using a vibrating-beam technique, determined the relationship between the density (ρ) and Young's modulus (E) for Greenland snow. Since the velocity at which elastic waves propagate (c_0) is related to Young's modulus by the formula $c_0 = \sqrt{\frac{E}{\rho}}$, c_0 can be calculated from Nakaya's data. For the snow studied here the values shown in Table IV were calculated.

The values of c_0 calculated from vibration tests, for snow density greater than 0.5 g/cm^3, are generally higher than the values determined from streak records of impact experiments (Fig. 7). This is not surprising since Nakaya found the velocity of propagation decreases with increase in frequency, and in the impact problem all frequencies are present. The data used to calculate the c_0 in Table IV were based on measurements at rather low frequencies of between 200 and 300 cps. Nakaya studied the frequency dependence of Young's modulus in the range of from 150 to 600 cps, and in this range he observed the decrease in Young's modulus with increase in frequency.

However, neglecting the frequency effect we can easily calculate, at least for the elastic wave, the percent deviation in c_0 as a function of the variation in density. Nakaya found the following relationship to hold between E and ρ for $\rho > 0.5$ g/cm^3: $E = (16.4\rho - 7.20) \times 10^{10}$ dynes/cm^2 or $E = a\rho - b$. We can calculate the percentage error in c_0 for a given error, or deviation in ρ, by first taking the logarithm of eq 5 and then taking the derivative.

$$\text{Since } c_0^2 = E/\rho \text{ or } \rho(c_0)^2 = E \tag{5}$$

$$\log \rho + \log c_0^2 = \log E = \log(a\rho - b)$$

$$\frac{d\rho}{\rho} + \frac{2dc_0}{c_0} = \frac{dE}{E} = \frac{ad\rho}{a\rho - b} \tag{6}$$

$$\frac{dc_0}{c_0} = \frac{1}{2}\,\frac{d\rho}{\rho}\left(\frac{b}{a\rho - b}\right) . \tag{7}$$

To illustrate the use of this equation, the percent deviation in density from the mean value of density of old Peter snow* is $\pm$ 3%. Therefore, from eq 7 the percent variation in c_0 is

*Peter snow is snow that has been disaggregated and deposited by the Peter snow miller.

$$\frac{dc_0}{c_0} = \frac{1}{2}(3)\frac{7.2 \times 10^{10}}{1.08 \times 10^{10}} = 11\%$$

or $\pm$ 11% error in c_0 for a $\pm$ 3% deviation in density.

The function $E = a\rho - b$ determined by Nakaya was based on data which itself exhibited a deviation of between 15 and 30%.

The sensitivity of the plastic-wave velocity to variations in the original density is not known, but we should expect that with increase in pressure the effect of variations in density would decrease.

The influence of variations in permeability. The measured values of permeability for the various snow types are listed in Table III. Although there is scatter in these values for any one snow type, this is not as significant as the implied relationship between density and permeability for all snow types investigated. Although we should expect a decrease in permeability with increase in density, the data show the opposite trend. The values of permeability for TWH-16 and TWH-23 lie within the range determined by Waterhouse (personal communication) at the M site (a quartermaster installation near Site II in Greenland) in 1960. The permeability of snow types MH-8, TWH-16, and NP deviate considerably from the expected values and must be considered in error. Thus, conclusions regarding permeability as a parameter cannot be drawn since we consider our initial data inaccurate.

The effect of orientation of the snow core. For the two snow pairs investigated (TWH-16, TWV-16 and TWH-23, TWV-23), there seems to be less scatter in the data for horizontal cores. The P-V curves indicate in both of these cases that the vertical cores yielded at lower pressures and also compacted more than did the horizontal cores from the same depth. What is rather interesting is that the P-V curves and the particle velocity-wave velocity curves show that the vertical and horizontal cores from a 16-ft depth give almost identical results, while for those from a 23-ft depth there is a large difference between the curves for horizontal and vertical orientation. Yet the densities of TWH-23 and TWV-23 were almost identical, while there was a large difference in the densities of TWH-16 and TWV-16. Thus it is not realistic to generalize as to the influence of this parameter on the overall material response.

The effect of temperature variations. Nakaya (1959) and Yosida (1956) found that Young's modulus for snow depends not only on density but also upon temperature. Yosida studied the dependency of E on temperature (consequently we can deduce the dependency of c_0 on temperature) for snows of density 0.29, 0.33, and 0.54 g/cm^3. For a given density of snow a decrease in temperature causes an increase in Young's modulus. For snow of density 0.630 g/cm^3, a temperature spread of from -10 to -20C results in a total variation of E of about 23% (Nakaya, 1959). Using eq 6 we calculate that this variation in E resulting from a 10-deg difference in temperature results in an 11% variation in the value of c_0.

The temperature in the trench where experiments were conducted was recorded before each experiment. These values are found in Table II. The variation in the recorded temperature for any snow type should give some indication of the extent to which the scatter in the results can be attributed to the temperature sensitivity of the material.

The cold room where the samples were prepared prior to testing was warmer than the trench. We have insufficient knowledge of the effect this temperature cycling would have on the material response.

The effect of variations in the initial loading conditions. Previous experience with a similar experimental procedure has shown that we can expect about a 5% variation in input loads for apparently identical initial loading conditions. However, even if the experiment were less reproducible than this, it would not affect results since all quantities used in calculations are measured directly from the streak records and none of the initial input information, except, of course, the initial density, is used.

BLANK PAGE

Table III. Actual measured values of density and permeability for three samples of each snow type.

Snow type	Density (g/cm^3)	Avg density (g/cm^3)	Permeability (cm/sec)	Avg permeability (cm/sec)
TWH-23	0.524 0.528 0.532	0.528	60 56 58	58
OP	0.482 0.512 0.522	0.505	63 99 78	80
NP	0.492 0.500 0.506	0.499	45 29.7 36	37
TWH-16	0.506 0.510 0.520	0.512	90 81 84	85
MH-8	0.376 0.392 0.396	0.388	68 17 20	18.5 or 35
TWV-23	0.524 0.530 0.532	0.529	34 28.5 28	30
TWV-16	0.458 0.468 0.472	0.466	18 17.5 17.3	17.6

Table IV. Elastic-wave velocity as calculated from Young's modulus.

Snow type	Avg density ρ_0 (g/cm^3)	Young's modulus* E ($dynes/cm^2$)	Elastic-wave velocity $c_0 = \sqrt{E/\rho_0}$ (cm/sec)
TWH-23	0.528	1.46×10^{10}	1.66×10^5
OP	0.505	1.08×10^{10}	1.46×10^5
NP	0.499	0.96×10^{10}	1.38×10^5
TWH-16	0.512	1.20×10^{10}	1.53×10^5
MH-8	0.388	0.23×10^{10}	0.76×10^5
TWV-23	0.529	1.47×10^{10}	1.66×10^5
TWV-16	0.466	0.355×10^{10}	0.87×10^5

*From Nakaya, 1959

BLANK PAGE

Errors in the data-reduction process

The errors associated with the data-reduction process can be severe. The greatest error occurs as a result of measuring angles in order to calculate velocities. The percentage error in the value of the tangent of an angle is greatest when the angle is near 0 or 90 deg. The slope of the elastic wave is generally near 80 deg on our test records, and the plastic-wave slope is usually less than 60 deg. Consequently, an error in measurement of the slope of the plastic wave results in a smaller percentage error in the value of its tangent as compared to the elastic wave, and hence there is a smaller error in the calculated plastic-wave velocity than in the elastic-wave velocity.

The following calculation shows how we can estimate the magnitude of the error in determining elastic- and plastic-wave velocities. Let

$$U_s = k\tan\theta \ .$$

Where:

U_s = the wave velocity

k = a constant

θ = the angle the wave makes with the horizontal

$$\log U_s = \log k + \log\tan\theta$$

$$\frac{dU_s}{U_s} = \frac{d\tan\theta}{\tan\theta} = \frac{2d\theta}{\sin 2\theta} \ . \qquad (8)$$

Thus, using eq 8, if U_s = 80 deg, and there is an uncertainty in measuring its value of 2 deg, the percentage error in the calculated value of elastic-wave velocity is 20%. When U_s = 85 deg, and $\Delta\theta$ = 2 deg, the error in wave velocity is 40%. This error is noticed most on the P-V curves at the lower pressures since it is the elastic wave which gives the greatest contribution.

However, when we consider the plastic wave, the minimum error would occur at 45 deg and the maximum error at 60 deg or 30 deg. Using eq 8, we find that for a $\Delta\theta$ = 2 deg the minimum error is 7% and the maximum error is about 8%.

Errors associated with neglecting geometry changes

The extent of the lateral deformation can be seen in the framing photographs, record numbers 165, 166, 169, and 170. The time between frames for each of these records is about 250 μsec and the exposure time is about 55 μsec. The P-V data were determined by measurements made on the streak records, and were limited to early times only, thus the lateral expansion of the snow should not seriously affect results for the low-pressure work. However, since no framing pictures were taken at the higher pressures, we cannot reliably extrapolate these observations to the high-pressure experiments. The P-V curves as well as the information listed in Table II show that the material is compacted to a very high density, at moderate pressure levels. If more framing records were available we might be better able to correct this density value and obtain a more realistic value.

CONCLUSIONS AND RECOMMENDATIONS

The streak camera records obtained on this program indicated that the technique used is valid for obtaining data on the impact response of snow and could also be applied to pressures even higher than those obtained here. The general features of the P-V curves are similar in form to those for other porous, crushable materials (Zaker,

1960, 1961; Stesau and Napadensky, 1962; Austing, 1960). First the material behaves elastically until the yield point is reached, then crushing or compaction occurs (i.e., a large volume change for a small change in pressure); next there is a region of relatively small compression or volume change for a large pressure change until finally a limiting density (presumably that of ice) is reached.

The limited number of experiments conducted on Michigan snow of density 0.5 g/cm^3 indicates that this material behaves somewhat differently than Greenland snow of the same density. It compacts considerably less than Greenland snow. The Michigan snow was about -23C prior to testing; the Greenland snow was not that cold.

The instrumentation in its present form is of limited value for studies on ice at these same pressure levels. It was not possible to analyze the streak camera records for ice (Napadensky, 1962) because the wave-propagation velocity is so fast that it appears as a vertical line on the film record. Even if we were to increase the film speed so as to accurately resolve the wave velocity, there would be a large error in measuring the particle velocities. This is because the ratio of wave velocity to particle velocity for ice, for pressures up to several hundred atmospheres, is about 50 to 1. If, however, photographic observations were made with two cameras operating simultaneously, but each operating at different speeds, we could resolve the wave speed with one camera and particle speeds with the second camera.

Our analysis indicates that at pressures of the order of 100 atm, snow is compressed to a density approaching or even exceeding ice. This is, in fact, highly unlikely at these pressure levels. The several sources of errors account in part for the high values of density. If, however, high-speed framing pictures were taken simultaneously with streak pictures we could determine the radial expansion of the material as it is being compressed, for each test, and thus could calculate a more realistic value of density or volume change.

To minimize the scatter in the data, further experiments should be conducted under very closely controlled environmental conditions. A constant temperature should be maintained and temperature cycling should not be permitted. Reproducibility in physical properties is a condition seldom found in natural media; however, carefully prepared Peter snow is expected to have the least sample to sample variation. (Although Landauer (1955) has found deviations of 10 to 20% on uniaxial compression tests on carefully sifted snow performed at temperatures that were controlled within ±0.5C.) Samples for dynamic experiments should be selected for uniform properties by measuring the density, porosity, and permeability of each sample. From the apparently uniform specimens selected, several samples should be tested under static unconfined compression. The remainder of the samples should be tested dynamically. Now that we have a general indication of the behavior of different snow types, future effort should be concentrated on obtaining more precise data for fewer materials.

It would be of much interest to observe the microstructure of the material both before and after impact. Sample recovery can be accomplished by a slight modification of the present experimental technique, i.e., by using a driver plate that is several times the diameter of the snow sample and surrounding the snow with a fiberboard container shorter than the sample. This driver-plate stop has proved effective in preventing the plate from pulverizing the test material under study. The microscope work should also give additional information as to the density of the compressed snow. Microstructure studies in conjunction with the impact experiments should indicate how the structure of the material is changed as a function of applied load.

REFERENCES

Anderson, D. C. (1962) Recommendations for employment of atomic demolitions, Armour Research Foundation Phase Report on Project D195 for U. S. Army Corps of Engineers, Engineer Research and Development Laboratories.

Austing, James L., et al. (1960) Strong shocks in porous media, Proceedings of Third Symposium on Detonation, James Forrestal Research Center, Princeton University, September 26-28, vol. 2, Office of Naval Research Symposium Report ACR-52, Washington, D. C.

Chaszeyka, M. A. (1961) Studies of surface and underground nuclear explosions, Armour Research Foundation Final Report on Project D195 for U. S. Army Corps of Engineers, Engineer Research and Development Laboratories.

_____ and Porzel, F. B. (1958) Study of blast effects in soil, Armour Research Foundation Final Report on Project D119 for U. S. Army Corps of Engineers, Engineer Research and Development Laboratories.

Landauer, Joseph K. (1955) Stress-strain relations in snow under uniaxial compression, Journal of Applied Physics, vol. 26, no. 12, p. 1493-1497.

Nakaya, Ukichiro (1959) Visco-elastic properties of snow and ice in the Greenland Ice Cap, U. S. Army Snow, Ice and Permafrost Research Establishment, Corps of Engineers, Research Report 46.

Napadensky, H. S. (1962) Dynamic response of snow to high rates of loading, Armour Research Foundation Data Report on Project D246 for U. S. Army Corps of Engineers, Cold Regions Research and Engineering Laboratory.

Office of the Secretary of Defense Research and Engineering (1961) Shock, vibration and associate environments, Part III, Bulletin no. 29, Washington, D. C.

Stresau, R. H., and Napadensky, H. S. (1962) Observation and measurement of behavior of porous materials when rapidly compressed, Experimental Mechanics, vol. 2, no. 1, p. 15-22.

Yosida, Zyungo, et al. (1956) Physical studies on deposited snow II, mechanical properties, Contributions from the Institute of Low Temperature Science (Hokkaido University, Sapporo, Japan), no. 9, p. 1-81.

Zaker, T. A. (1960) Studies of reactor containment, Armour Research Foundation Summary Report no. 3 on Project D132 for the U. S. Atomic Energy Commission.

_____ (1961) Studies of reactor containment, Armour Research Foundation Summary Report no. 4 on Project D132 for the U. S. Atomic Energy Commission.

BLANK PAGE

APPENDIX A.
EXPERIMENTAL PROCEDURES

CONTENTS

	Page
Test area description	A1
Experimental techniques	A1
Explosive initiation system	A3
Grid lines on snow	A3
Grid lines on driving plates	A3
The streak camera	A3
Synchronization of camera and event	A3
Synchronization of flash bulb and event	A4
Timing-light generator	A4
High-speed framing camera	A4

ILLUSTRATIONS

Figure		
A1.	Camp Century —plan view	A2
A2.	ARF work areas at Camp Century — plan view	A5
A3.	Experimental arrangement at Camp Century	A6
A4.	Same experimental arrangement at ARF explosives laboratory	A6
A5.	Vacuum removal of film chips from camera	A7
A6.	Photograph of work bench, insulated box, and warning siren	A7
A7.	High-explosive magazine	A8
A8.	Engineer activating firing switch	A8
A9.	Fire and smoke during an actual experiment	A9
A10.	Test specimen mounted between anvil and driving plate	A9
A11.	Assembly mounted in fragment and smoke shield	A9
A12.	Cutaway perspective view of test assembly	A10
A13.	Device for scribing driving plate	A11
A14.	Firing delay circuit	A11

APPENDIX A: EXPERIMENTAL PROCEDURES

TEST AREA DESCRIPTION

The exact location in the Camp Century trench network of the Armour Research Foundation test area is shown in Figure A1. Details of the ARF work area can be seen in Figure A2. The primary facilities used on this program were a location for the test fixture and camera, ready magazines for the explosives, a work table in an unheated area for assembly of test components, an insulated storage box near the work bench, a dark room for film processing, a heated workshop, and a cold laboratory for sample preparation.

The massive steel test fixture, in which the samples to be tested were placed, was supported on a wooden platform about 4 in. thick, which rested on the snow floor of the trench. The base of the platform was sprayed with water, and thus the whole unit was rigidly frozen in place. The primary function of this test fixture was to shield the camera's field of view of the impacted specimen from the smoke and fire associated with the initiation of the driving-plate charge. The purpose of the long anvil in the test fixture was to permit sufficient time for the event to be completed within the double transit time of any waves which might propagate through the anvil.

The camera tripod was also frozen in place on the floor of the trench. The camera was kept warm by an electric heating pad wrapped around it, which was covered with heavy-duty aluminum foil and taped in place with M&M masking tape or household freezer tape. The electronic equipment was kept under a plastic tarp to protect it from falling hoarfrost and frost formation. The test setup is shown in Figures A3 and A4.

The vacuum cleaner seen in Figures A3 and A5 was used to remove chips of broken film remaining in the camera after each shot. A barricade of snow blocks was placed along two sides of the equipment (perpendicular to the trench wall) as a safety precaution. Figure A3 shows remains of a snow barricade after many shots.

The workbench used for assembling the inert parts, as well as serving as a desk for making logbook entries, was at one end of the trench. The table was made by placing a 0.5-in. plywood sheet into saw cuts in the corner of the snow walls. The free corner was supported on blocks of snow. A box for ready access and warm storage of certain inert parts needed near the work table was built from 2-in. Styrofoam planks and heated with two heating pads. This area can be seen in Figures A2 and A6.

A limited amount of explosives needed for the tests (powdered tetryl for the main charge and pressed-tetryl pellets for the booster) was kept in one magazine. The blasting caps (detonators) were kept in a separate magazine. The location of those items is seen in Figure A2. The magazines were made by cutting out a block of snow, at a convenient height, and using the cavity for storage. The block of snow was then put back in place to serve as a cover. Figure A7 is a photograph of one of the magazines. The remainder of the explosives was stored topside.

The firing switch box (Fig. A8) sent an electrical signal to fire the detonator and actuate the camera. Before throwing the switch, a warning blast from a siren was sounded to alert anyone in the vicinity of the impending explosion. Figure A9 is a photograph, taken from one end of the tunnel, of the explosion during an actual test.

EXPERIMENTAL TECHNIQUES

In this experiment, the pressure-volume relationships for the material being studied are acquired by a series of experiments arranged as shown schematically in Figure 3 of the report. Figures A10 and A11 are photographs of the apparatus, showing various stages of assembly, and Figure A12 is a detailed drawing of the setup.

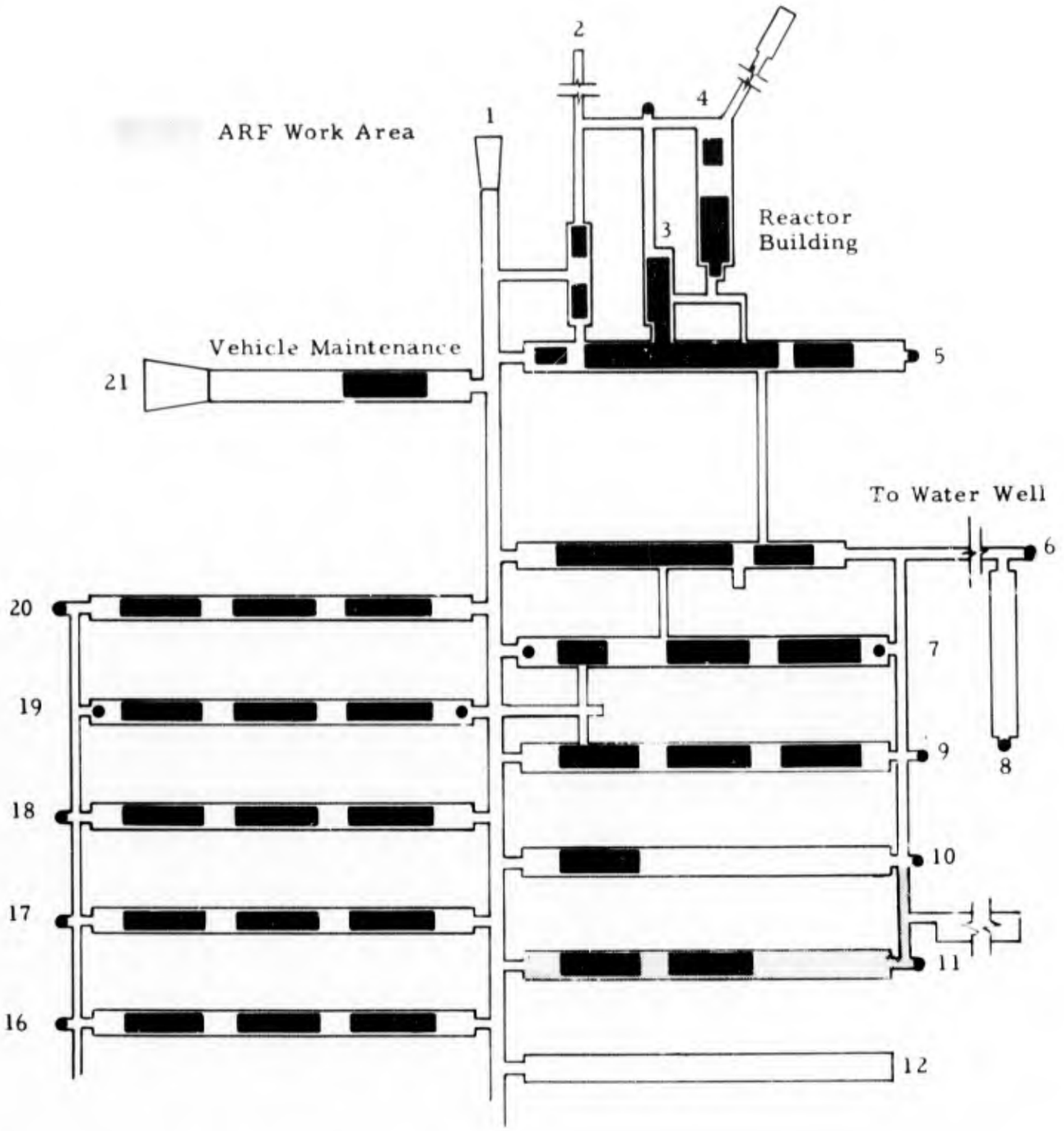

Figure A1. Camp Century — plan view.

Explosive initiation system

Figure A12 is a schematic drawing showing the initiation system of the explosive charge. It is the initiation of the powdered tetryl explosive almost simultaneously over its surface that results in the driving plate being uniformly accelerated. This initiation is accomplished by the fragmentation of the aluminum strip when a contiguous booster is ignited by a blasting cap. The fast-flying, hot aluminum fragments strike the tetryl explosive main charge in a large number of places simultaneously and detonate it.

Grid lines on snow

Several techniques were used for painting grid lines on snow. The technique which seemed to give the best results utilized from three to five superimposed layers of paper stencils. Horizontal stripes, corresponding to stripes on the snow, were cut into the stencil paper. The stripes in each layer were progressively thinner, the thinnest being on the stencil closest to the snow sample. The thinnest slits (beginning with shot no. 67) were 1/16-in wide on 1/8-in. centers. The table of log book entries should be consulted for the dimensions of the stripes for those tests prior to shot no. 67. The actual stripes on the snow were obtained by spraying the snow, through the stencils, with black Krylon (spray can). A small amount of Krylon was sprayed on at a time and was permitted to freeze before the next application. Three coats of Krylon were generally adequate. Satisfactory results were also obtained using black Derusto paint in a spray can.

Grid lines on driving plates

Bright lines on a black background were made on the driving plates by first spraying the plates with Derusto paint. Before the paint was dry, the plate was put into the scribing device (Fig. A13), and the serrated knife-edges of the scribe were moved across the plate. This action removed the paint so that a series of fine lines was exposed on the actual metal surface of the plate. The lines on all plates are 0.025-in. wide on 0.100-in. centers.

The streak camera

The streak camera used in these experiments was a Wollensak 35 mm Fastax in which the rotating prism was replaced by a stationary slit plate. The slit plate was made from two pieces of 0.005-in. steel shim stock-mounted on a frame. The slit opening of 0.010 in., combined with a film transport of 2 in. per msec, resulted in a film exposure time of about 5 μsec.

The camera was adapted to give image-to-object size ratios of 1/1 and 1/2 by the use of extension tubes with a 6-in. telephoto lens. The long focal length was used to attain a reasonable stand-off distance for protection of the camera at these ratios.

The film used for all the photographic records was Kodak Tri-X, TXN-415 in 100-ft rolls. The film was processed by developing it for about 8 min in Eastman D-11 developer, and then fixing it with Edwal Quikfix and Edwal hardener. The Quikfix was mixed in ratio of 4 parts water to 1 part Quikfix concentrate, plus 4 oz hardener to 1 gal of mix.

The reflectors, used with the GE no. 31 focal plane flash bulbs, were made of heavy-duty aluminum foil. After each shot, the flash bulb and reflector were both thrown away.

Synchronization of camera and event

For this study, the camera had to be synchronized with the event. Also, since the film speed is determined by the input voltage, a camera speed control was necessary. To satisfy these requirements, the Wollensak "Goose" Control Unit was used. This unit incorporates both a variable a-c voltage control and a set of timers for controlling the relationship between the event and the camera. For this application, the camera was started 0.6 sec before the detonator firing pulse.

APPENDIX A.

Synchronization of flash bulb and event

The specimen and driving plate were illuminated by means of a GE no. 31 focal plane flash bulb. The first impulse, of course, was to connect the detonator and the flash bulb in parallel or series. However, since it takes a flash bulb about 25 msec to reach its full intensity, most of the interesting action would have been over before it could be photographed with such an arrangement. The simple circuit shown in Figure A14 was used to delay the firing of the detonator until the flash bulb had reached its maximum intensity. The heating rate of the tungsten filament of an ordinary light bulb, combined with its high thermal coefficient of resistivity, provide the delay. When the filament is cold, its resistance is about 4 ohms so that the voltage across the detonator is about 1/150 of the Variac output (V_1). However, when the filament reaches its operating resistance of 70 ohms, the voltage across the detonator rises to about 1/50 of V_1.

A calibration of detonator firing time versus Variac setting was made with the help of a Berkeley Counter Chronograph. As might be expected, a time variation of about a half cycle (9.3 msec) was observed. This jitter is not excessive for the present use, because the brightness of the source is nearly constant for several times this period.

Timing-light generator

To record the rate of film travel reliably and accurately, a timing-light generator was used. This generator provided the time pip to the camera's neon lamp which marks or exposes the edge of the film. The 1-msec interval timing marks, used on all records for this program, were achieved by means of a 1000-cycle, crystal control oscillator incorporated in the timing-light generator.

High-speed framing camera

The framing camera used for some of the experiments was a 35 mm Wollensak Model WF8A. Although the accuracy of measurements from framing-camera pictures is usually not very high, such records often give qualitative information in a more rapidly assimilated form than do streak-camera records. The framing camera is an ideal means of observation when the event is two-dimensional.

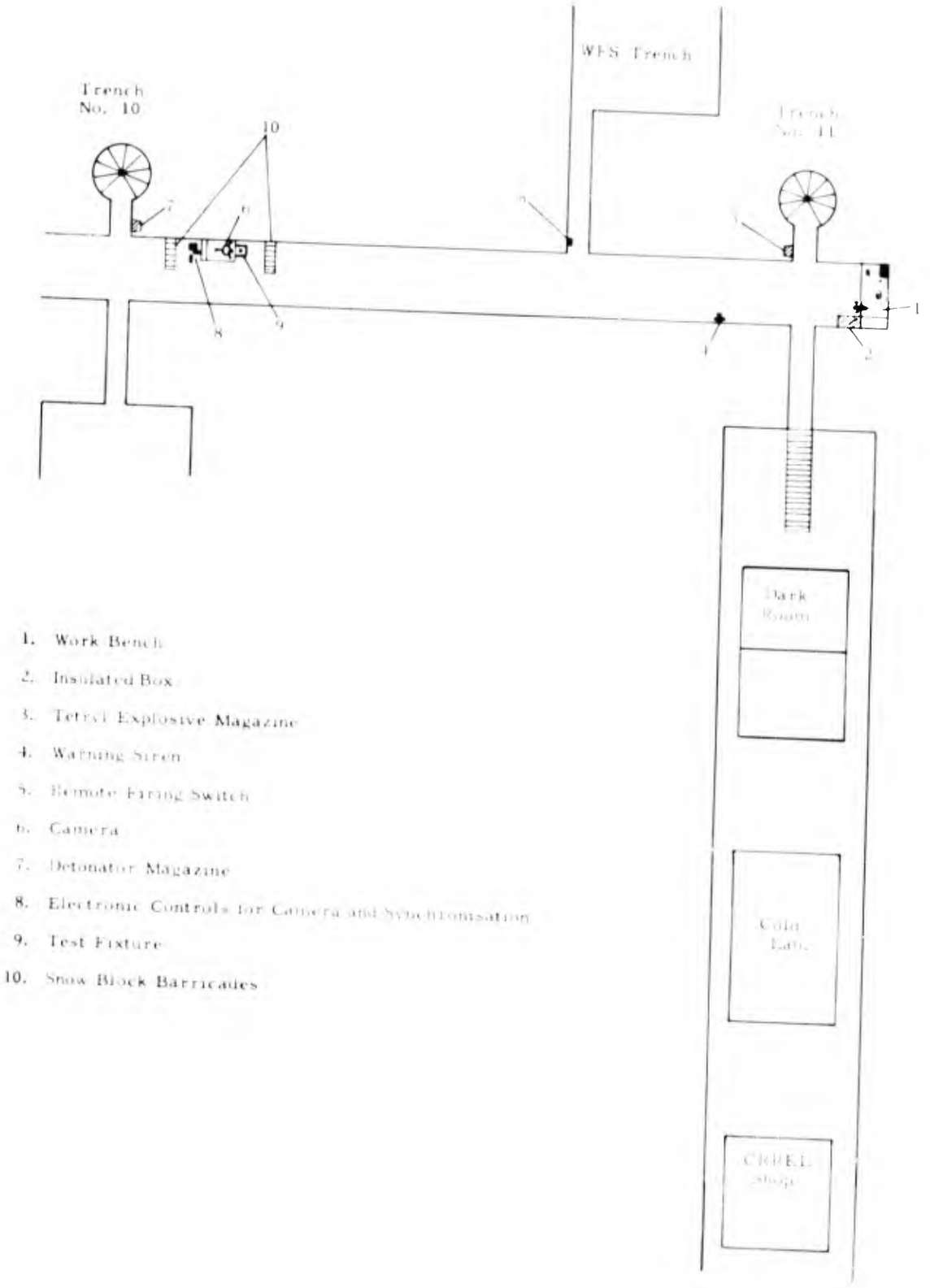

1. Work Bench
2. Insulated Box
3. Tetryl Explosive Magazine
4. Warning Siren
5. Remote Firing Switch
6. Camera
7. Detonator Magazine
8. Electronic Controls for Camera and Synchronization
9. Test Fixture
10. Snow Block Barricades

Figure A2. ARF work areas at Camp Century — plan view.

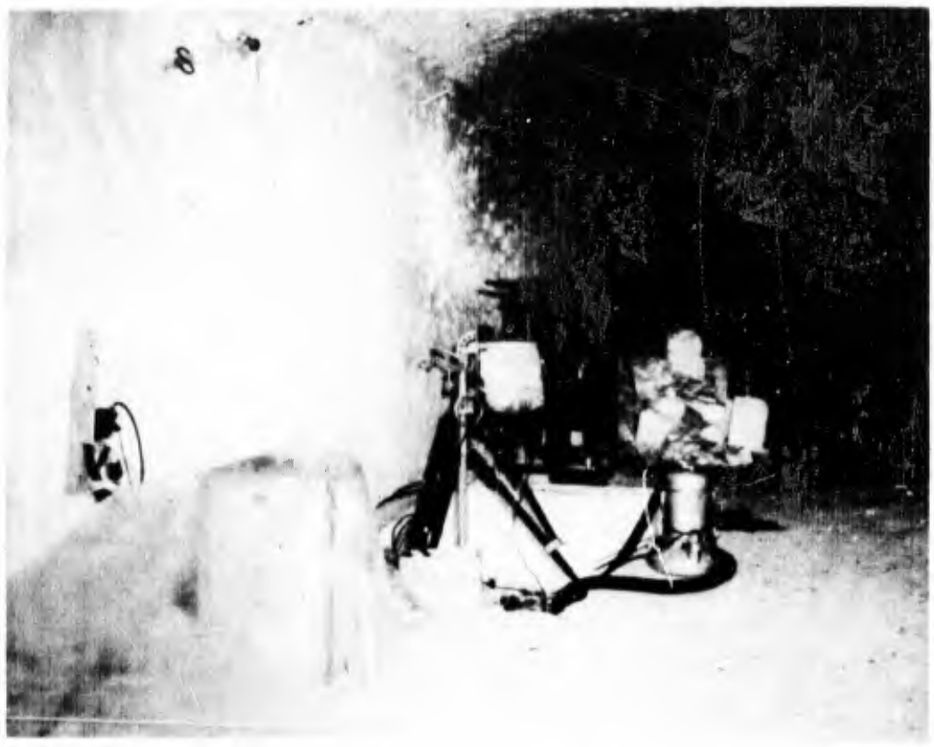

Figure A3. Experimental arrangement at Camp Century.

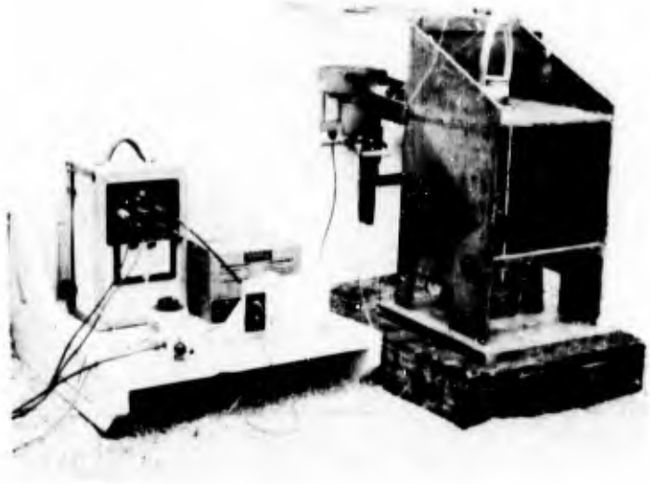

Figure A4. Same experimental arrangement at ARF explosives laboratory.

BLANK PAGE

Figure A5. Vacuum removal of film chips from camera.

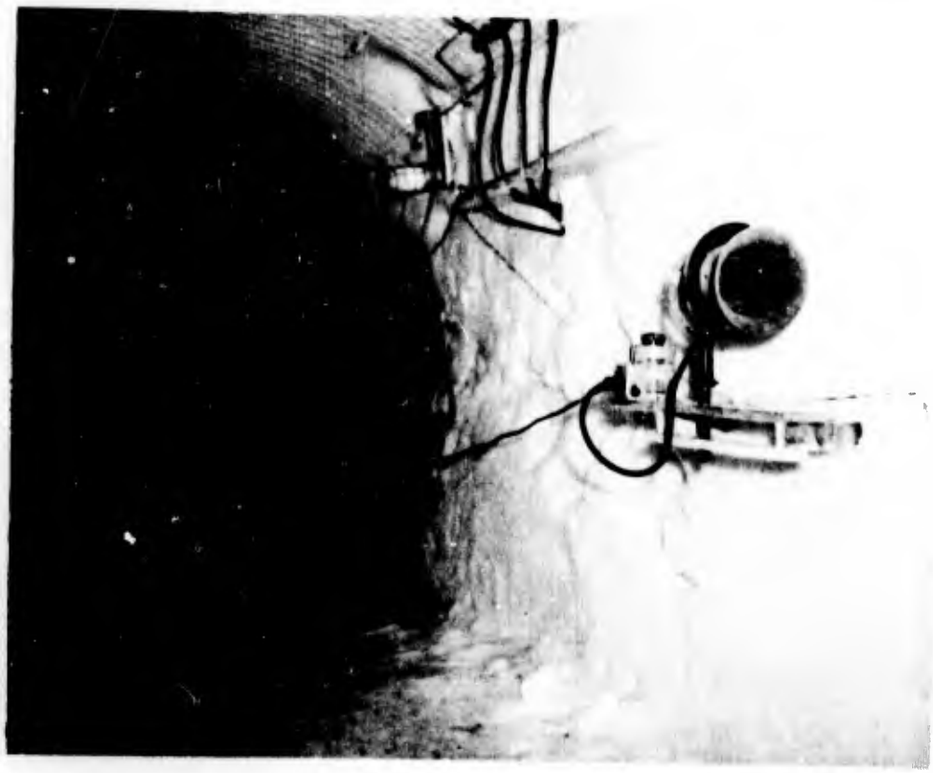

Figure A6. Photograph of work bench, insulated box, and warning siren.

Figure A7. High-explosive magazine.

Figure A8. Engineer activating firing switch.

BLANK PAGE

Figure A9. Fire and smoke during an actual experiment.

Figure A10. Test specimen mounted between anvil and driving plate.

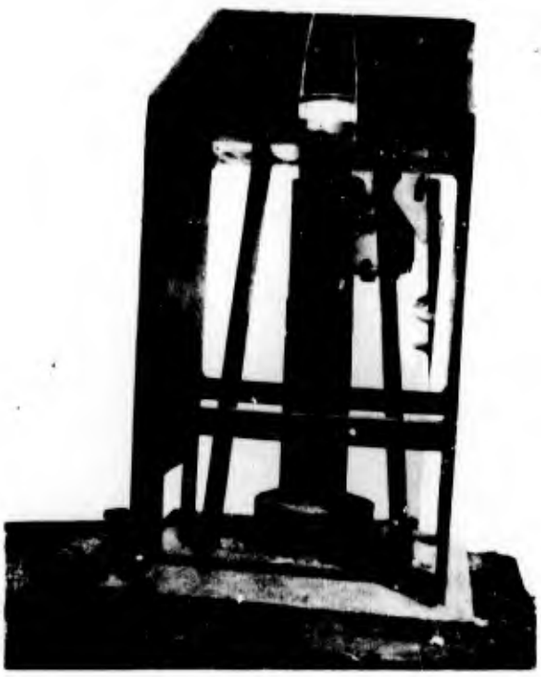

Figure A11. Assembly mounted in fragment and smoke shield.

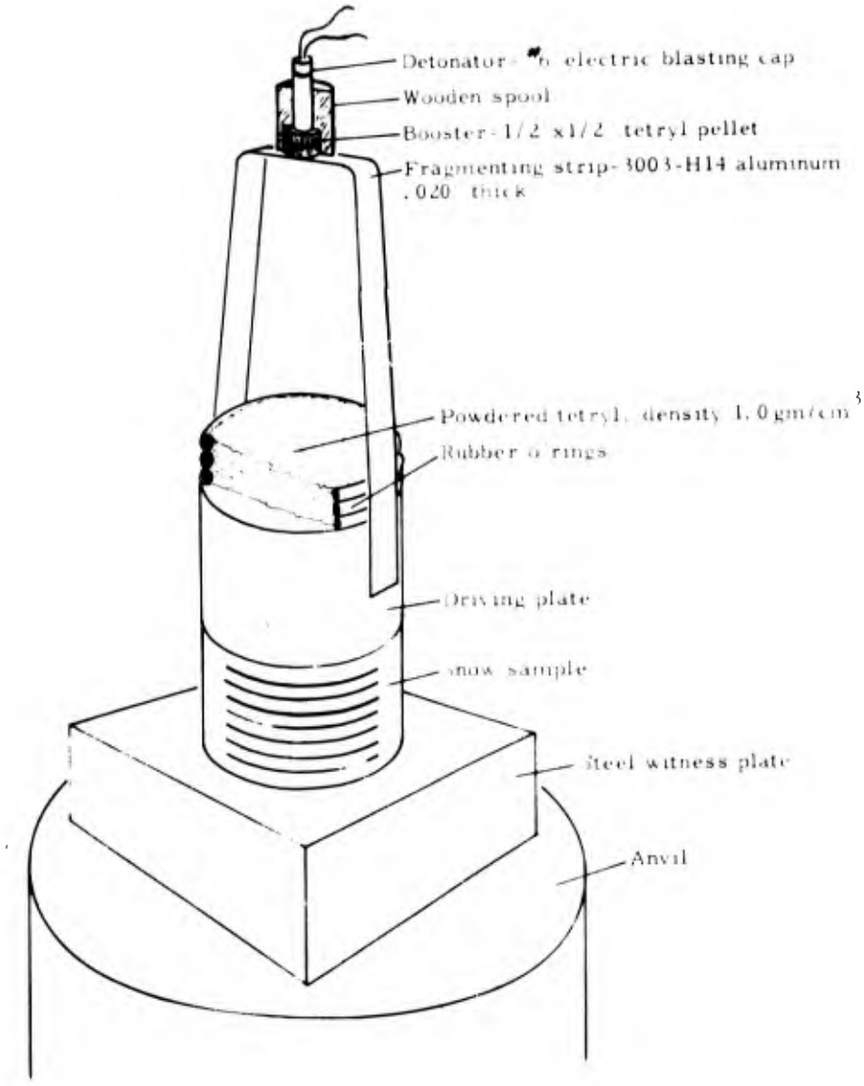

Figure A12. Cutaway perspective view of test assembly.

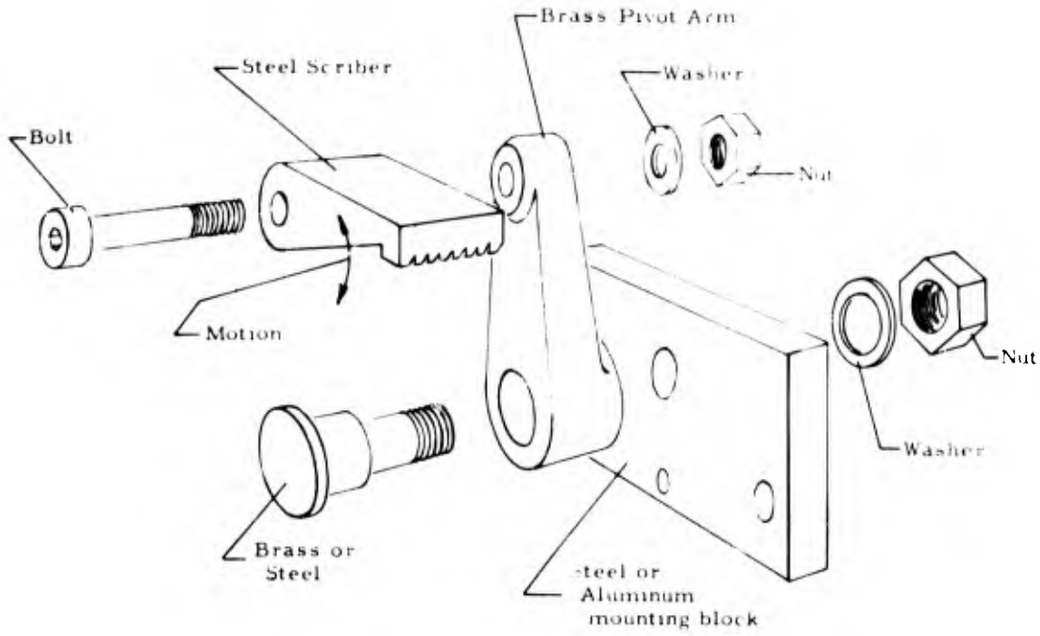

Figure A13. Device for scribing driving plates.

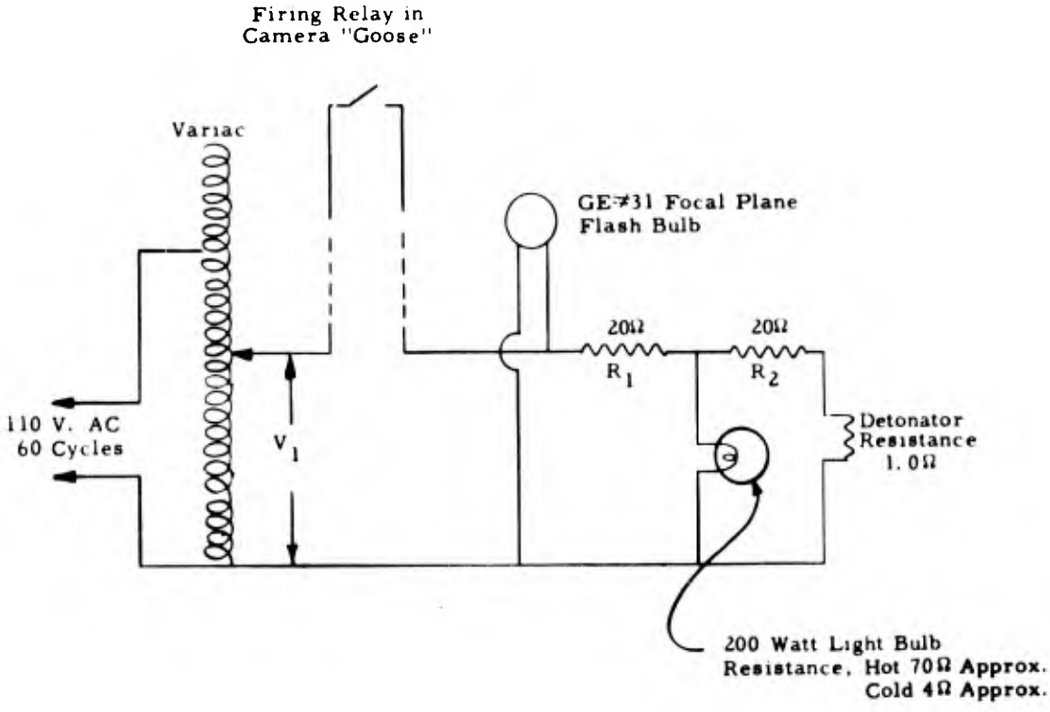

Figure A14. Firing-delay circuit.